Link between Protein−Solvent and Weak Protein−Protein Interactions Gives Insight into Halophilic Adaptation†

Lionel Costenaro,‡,§ Giuseppe Zaccai,‡,|| and Christine Ebel*,‡

LBM, Institut de Biologie Structurale, UMR 5075 CEA-CNRS-UJF, 41 rue Jules Horowitz, 38027 Grenoble, France, and Institut Laue-Langevin, 6 rue Horowitz, 38000 Grenoble, France

Received March 18, 2002; Revised Manuscript Received August 30, 2002

ABSTRACT: Malate dehydrogenase (*Hm* MalDH) from the extreme halophile *Haloarcula marismortui* is a very acidic protein with extensive ion binding properties. It is a good model for the study of solvation−solubility relationships. We measured the small-angle neutron or X-ray scattering profiles of folded and stable *Hm* MalDH at various protein concentrations and derived the second virial coefficients A_2. In NaCl, CsCl, KF, KCl, and $NaCH_3CO_2$, A_2 values are positive, indicating globally repulsive protein−protein interactions. Below 1 M $MgCl_2$ and $MgSO_4$ or above 2 M $(NH_4)_2SO_4$, A_2 rapidly decreases. From structure factor modeling with DLVO (Derjaguin, Landau, Verwey, and Overbeek)-like potentials, an effective diameter of 80−82 Å is found for the protein particle in solution, compatible with its structural dimensions; the effective charge of the particle is undefined because of the high salt concentration. The strong variations of the protein−protein interaction are correlated to an attractive potential whose depth evolves with the salinity but in an opposite way in Mg salts and $(NH_4)_2SO_4$. A repulsive Donnan term, corresponding to counterion dissociation, and an attractive term related to previously measured preferential salt binding parameters are discussed from well-established thermodynamics considerations and qualitatively account for the behavior of the protein−protein interactions in the various solutions. Because a solvation shell with a composition different from bulk induces protein−protein attraction, molecular adaptation to high salt would be directed to allow protein−salt interactions in order to avoid water or salt enrichment at the surface of the protein and thus preserve its solubility.

The cell is an extremely concentrated environment in which macromolecules remain soluble despite the molecular crowding. Biological functions can be operated by labile but specific large complexes. Weak protein−protein interactions modify the rates, equilibrium, and mechanisms of reactions (*1*). They control the spatial distribution of proteins in solution and determine their capacity to remain soluble, form an amorphous precipitate, or crystallize. The study of weak protein−protein interactions explained the transparency of crystalline lens (*2*, *3*) or described the crystallization capability of proteins (*4*−*8*).

The aim of the present study is to relate protein−solvent interactions to weak protein−protein interactions. In the companion article (*9*), we have investigated the protein−solvent interactions of malate dehydrogenase (*Hm* MalDH[1]) from the extreme halophile *Haloarcula marismortui* in a variety of salts, including NaCl, $(NH_4)_2SO_4$, and $MgCl_2$. *Hm* MalDH is a 130 kDa homotetramer extremely rich in acidic residues with an excess of 156 negative charges (pI 4.5). The results, interpreted in terms of strong solvent binding sites, give an amount of solvating water varying by a factor of 2, from 2000 to 4100, and bound salt between 0 and about 85 mol per mole of protein, depending on the salt conditions. Because of its exceptional and diverse solvation properties, *Hm* MalDH is a good model for our purpose. The second virial coefficient A_2, which is related to weak protein−protein interactions, was shown for *Hm* MalDH to evolve strongly and in a complex way with the salt type and concentration (*10*), and also in the presence of organic solvent, in a study on the protein crystallization (*11*).

In the present paper, we extend these recent studies. We measure the neutron or X-ray scattering profiles of *Hm* MalDH in a variety of salt conditions at different protein concentrations. From these measurements, we derive the second virial coefficients and the solution structure factors S, which are related to the spatial distribution of the macromolecules in the solution, and can be modeled with intermacromolecular DLVO (Derjaguin, Landau, Verwey, and Overbeek; *12*, *13*)-like potentials. We use well-established thermodynamics to relate the second virial coefficient and the preferential salt binding parameter, and we emphasize that a solvation shell with a composition different from bulk provide an effective protein−protein attraction contribution of entropic origin. The biological implications are discussed in term of molecular adaptation

† This work was supported by the CNES (Décision 793/2001/CNES/8860) and the CNRS (GEOMEX).

* Corresponding author. Tel: (33) 4 38 78 96 38. Fax: (33) 4 38 78 54 94. E mail: Christine.Ebel@ibs.fr.

‡ Institut de Biologie Structurale.

§ Present address: Biological Chemistry Dept., John Innes Centre, Colney Lane, Norwich NR4 7UH, U.K.

|| Institut Laue-Langevin.

[1] Abbrevations: *Hm* MalDH, Malate dehydrogenase from *Haloarcula marismortui*; DLVO, Derjaguin, Landau, Verwey, and Overbeek.

10.1021/bi025830z CCC: $22.00
Published on Web 10/11/2002

to high salt. The physiological medium of *Hm* MalDH is indeed very concentrated in salt as the extreme halophilic *archaea* accumulate intracellular KCl close to saturation to balance the very high external salt concentration of their biotopes.

THEORETICAL BACKGROUND

The Second Virial Coefficient. The osmotic pressure Π can be expanded in powers of the concentration c (in mg/mL) of a macromolecule of molar mass M_2 as

$$(d\Pi/dc)/N_A kT = 1/M_2 + 2A_2c + 3A_3c^2... \quad (1)$$

N_A is the Avogadro number, k the Boltzmann constant, and T the absolute temperature. A_2 is the second virial coefficient and A_3 the third, neglected at moderate concentrations. For weakly interacting quasispherical particles, A_2 is related to the pair interaction potential of mean force $W(r)$ and to the pair distribution function $g(r) = \exp(-W(r)/kT)$, where r is the interparticle distance (*14*)

$$A_2 = 2\pi N_A/M_2^2 \int (1 - e^{-W(r)/kT}) r^2 \, dr \quad (2)$$

Therefore, A_2 reflects the net protein−protein interactions. It is negative for globally attractive interactions and positive for globally repulsive interactions. It has to be noted that $W(r)$—and thus A_2—depends implicitly on all direct interactions between the solution molecules: macromolecules and also solvent components. A_2 can be evaluated from measurements providing the molar mass in solution (*15*−*17*).

The Structure Factor. The intensity $I(q,c)$ scattered by a solution of monodisperse spherical macromolecules can be expressed as

$$I(q,c) = I(q,0)S(q,c) \quad (3)$$

where $q = 4\pi \sin \theta/\lambda$ is the scattering vector and θ is half the scattering angle. $I(q,0)/c$, the form factor extrapolated from $I(q,c)/c$ at infinite dilution, is proportional to the mean intensity scattered by one macromolecule. $S(q,c)$, the structure factor, characterizes the intermolecular interactions. For an uncorrelated ideal system, $S(q,c) = 1$. $S(0,c)$, related to A_2, is lower than 1 for globally repulsive interactions and higher for globally attractive interactions. For quasispherical macromolecules, eq 3 is still valid within a smaller q range (*18*). The solution can be described mathematically as the convolution product of a particle shape by a particle distribution. $S(q,c)$ is the Fourier transform of the spherically averaged autocorrelation function of the particle distribution $g(r)$

$$S(q,c) = 1 + (c/N_A M_2) \int (g(r) - 1) e^{iqr} \, dr \quad (4)$$

Statistical mechanics allows to calculate $g(r)$ and $S(q,c)$ and A_2 values resulting from defined effective pair potentials $W(r)$, an approach that is extensively used in the field of colloid sciences (*14*, *19*).

Analysis in Terms of Intermolecular Potentials. In the DLVO model, the solvent is a continuum characterized by its dielectric constant ϵ and its ionic strength I (*12*, *13*). We used the following effective, ion-average, spherically symmetric pair potential $W(r)$

$$W(r) = \begin{cases} +\infty & \text{for } r \le D \\ \dfrac{kTZ^2 L_B}{(1 + \kappa D/2)^2} \dfrac{e^{-\kappa(r-D)}}{r} - JD \dfrac{e^{-(r-D)/d}}{r} & \text{for } r > D \end{cases} \quad (5)$$

The excluded-volume potential (first line) corresponds to the fact that macromolecules of effective diameter D cannot interpenetrate. The first term of the second line is the screened Coulombic potential, where Z is the effective charge of the protein. The screening constant $\kappa = (8\pi L_B I)^{1/2}$ is the inverse of the Debye length λ_D and related to the Bjerrum length $L_B = e^2/4\pi\epsilon_0\epsilon kT$, I being the ionic strength and ϵ_0 (ϵ) the vacuum (relative) permittivity. These two potentials are repulsive. The precise form of the attractive last term—for van der Waals or other attractions—is not important for short-range attraction described for macromolecules in aqueous solvent (*20*). We used a Yukawa potential with a positive depth J (in kT) and range d (in Å). For the second virial coefficient, the excluded-volume term $A_{2\,exc}$ is $4V_2N_A/M_2^2$, with V_2 being the solvated-protein volume, and the electrostatic part $A_{2\,elec}$ is $Z^2(1 + \kappa D)/(4IM_2^2(1 + \kappa D/2)^2)$.

Thermodynamic Analysis. Component 1 is water (the main solvent). Component 2 (subscript sometimes omitted) is the macromolecule, i.e., the *Hm* MalDH tetramer (polypeptide chains plus $|Z|/z_+$ counterions required for its electroneutrality with $|Z| = 156$). Component 3 is the salt composed of ν_+ cations X of charge $+z_+$ and ν_- anions Y of charge $-z$. Temperature is constant and subscript T omitted. The subscripts μ, m, and P signify constant chemical potentials of all diffusible components, constant molalities (mol/kg of water) of all components except the derived one, and constant pressure P, respectively. The chemical potential μ_i of component i is related to the molalities m_k of the included species k and to the excess chemical potential $N_A kT\beta_i$. β_i (the logarithm of the activity coefficient) is in general a function of pressure, temperature, and solution composition. β_i is related to all intermolecular interactions (*15*, *21*−*23*). Considering the dissociation of the Z/z_+ counterions and the macromolecule as well as of the $X_{\nu+}$:$Y_{\nu-}$ salt

$$\mu_2 = \mu_2^\circ + N_A kT \ln m_2 + (Z/z_+) N_A kT \ln(\nu_+ m_3 + (Z/z_+) m_2) + N_A kT\beta_2 \quad (6a)$$

$$\mu_3 = \mu_3^\circ + \nu_+ N_A kT \ln(\nu_+ m_3 + (Z/z_+) m_2) + \nu_- N_A kT \ln(\nu_- m_3) + N_A kT\beta_3 \quad (6b)$$

Considering a dilute solution of protein, $(Z/z_+)m_2 \ll \nu_+ m_3$, $a_{ij} = (\partial\mu_i/\partial m_j)_{P,m}/N_A kT$ reduces to

$$a_{22} = 1/m_2 + (Z/z_+)^2/(\nu_+ m_3) + \partial\beta_2/\partial m_2 = 1/m_2 + a_{22}^{\,D} + a_I^{\,22} \quad (7a)$$

$$a_{23} = (Z/z_+)/m_3 + \partial\beta_2/\partial m_3 = a_{23}^{\,D} + a_{23}^{\,I} \quad (7b)$$

$$a_{33} = (\nu_+ + \nu_-)/m_3 + \partial\beta_3/\partial m_3 \quad (7c)$$

The terms $a_{22}^{\,D}$ and $a_{23}^{\,D}$ are the Donnan terms related to the dissociation of the counterions of the macromolecule ($a_{23}^{\,D}$

was extensively discussed in the companion paper (*9*). a_{22}^{I} and a_{23}^{I} are nonideality terms from intermolecular interactions.

For a three-component system, the Gibbs−Duhem equation, dropping inconsequential terms, leads to (*15*, *21*, *22*)

$$d\Pi/dm_2 \equiv (\partial P/\partial m_2)_\mu \approx (N_A kT/V_m^0)(a_{22} - a_{23}^2/a_{33})m_2 + ... \quad (8)$$

When a_{22} is developed (eq 7a), eq 8 can be identified with the virial expansion (eq 1). The first virial coefficient, $1/M_2$ in eq 1, is related to a_{22} in eq 8, and more precisely to $1/m_2$ in eq 7a. The second virial coefficient A_2 can be expressed as $(\partial V_m/\partial m_2)_\mu^0/M_2^2 + (V_m^0/2M_2^2)(a_{22}^D + a_{22}^I - a_{23}^2/a_{33})$, or more simply as

$$A_2 = (\partial V_m/\partial m_2)_\mu^0/M_2^2 + A_{2\,22}^D + A_{2\,22}^I + A_{2\,23} \quad (9)$$

V_m and V_m^0 are the volumes of solution and solvent, respectively, containing 1 kg of water. The first term arising from concentration scale change is small and can be approximated as $\bar{v}_2/M_2$, $\bar{v}_2$ being the partial specific volume. The second term $A_{2\,22}^D = (V_m^0/2M_2^2)(Z/z_+)^2/(\nu_+ m_3)$ is one of the Donnan terms related to the dissociation of the macromolecule counterions (the second Donnan term from a_{23}^D is included in $A_{2\,23}$). The third term $A_{2\,22}^I = (V_m^0/2M_2^2)(\partial\beta_2/\partial m_2)$ arises from protein−protein interactions omitting the effects of counterion dissociation or solvent redistribution. In our analysis, we restrict this term to excluded-volume and electrostatic potentials. The last term $A_{2\,23}$ has an entropic origin and is related to the protein-induced solvent redistribution. Since $(\partial m_3/\partial m_2)_{\mu 3} = -a_{23}/a_{33}$, $A_{2\,23}$ is a function of the measurable preferential salt binding parameter $(\partial m_3/\partial m_2)_{\mu 3}$. $(\partial m_3/\partial m_2)_{\mu 3}$ is experimentally indistinguishable from $(\partial m_3/\partial m_2)_\mu$, and $A_{2\,23}$ can be expressed as

$$A_{2\,23} = -(V_m^0/2M_2^2)\, a_{33}\, (\partial m_3/\partial m_2)_\mu^2 \quad (10)$$

Since we consider the second virial coefficient, which is derived theoretically and experimentally for solutions at moderate or low protein concentration (some mg/mL), it is justifiable to neglect the influence of the protein in the calculation of a_{33}. We derived a_{33} by using the tabulated mean ionic activity coefficient $\gamma_\pm$

$$a_{33} = (\nu_+ + \nu_-)(1/m_3 + (\partial\gamma_\pm/\partial m_3)/\gamma_\pm) \quad (11)$$

For a sample at atmospheric pressure, the osmotic pressure obtained in a dialysis experiment corresponds to changes in μ_1 and μ_3. With $\bar{V}_i$ the partial molal volumes

$$\mu_{1\,or\,3} - \mu_{1\,or\,3\,bulk} = -\bar{V}_{1\,or\,3}\Pi = \bar{V}_{1\,or\,3}RT(-c/M_2 - A_2c^2 ...) \quad (12)$$

MATERIALS AND METHODS

Hm MalDH Solution. Hm MalDH was overexpressed in *Escherichia coli* and purified as in ref *24*, with a final gel filtration step in 4 M NaCl, concentrated, and stored at 4 °C. Extensive dialysis against the solvent of interest, buffered with 50 mM Tris-HCl pH 8, followed by weighted dilutions allowed to obtain protein concentrations of typically 7, 14, 21, and 60−100 mg/mL, measured using an extinction coefficient at 280 nm of 0.85 mL/mg/cm for the polypeptide chain.

Small-Angle Scattering. Neutron experiments were carried out on the instruments D11 and D22 of the "Institut Laue Langevin", ILL (Grenoble, France), in 1.00 mm path quartz cuvettes at controlled temperature. For D11/D22, the wavelength λ was 6 Å/10 Å ($\Delta\lambda/\lambda = 0.1$), the sample−detector distances 4.5 and 1.25 m/4 and 1.4 m with collimations of 5.5 and 13 m/of 8 and 11.2 m (with a detector offset of 0.382 m), respectively. The scattering levels of the protein solutions and corresponding solvent were when necessary corrected for small differences at $q > 0.28$ Å^{-1}. The small-angle X-ray scattering experiments were carried out at the "Laboratoire pour l'Utilisation du Rayonnement Electromagnétique", LURE (Orsay, France), on the D24 instrument, using a wavelength of 1.488 Å, a sample−detector distance of 1.82 m. For both type of scattering, the q-range was 0.01−0.3 Å^{-1}, the normalization procedures were usual, with correction for the detector efficiency for neutron scattering. Unless specified, measurements were at 20−25 °C.

Second Virial Coefficient Determination. We used, in a $R_g q$ range of 0.2−1.3, the Guinier approximation $\ln I(q,c) = \ln I(0,c) - R_g^2 q^2/3$ to extrapolate the forward intensity $I(0,c)$ and the radius of gyration R_g of the particle scattering density contrast (*25*). For ideal solutions, $I(0,c)/c$ is related to the molar mass M_2 (*16*, *26*, *27*) and, for real ones, to apparent values M_2^{app}. With three protein concentrations below 30 mg/mL, we obtained A_2 from the linear fit of $c/I(0,c)$ versus c: $c/I(0,c) = 1/I(0,0) + 2A_2M_2c/I(0,0)$.

Experimental Structure-Factor Determination and Structure-Factor Fitting. For each solvent condition, using the three lowest concentrated samples, the form factor $I(q,0)/c$ was obtained for q below 0.06−0.08 Å^{-1} by the linear extrapolation to $c = 0$ of $I(q,c)/c$ and, beyond $q = 0.08$ Å^{-1}, using the slightly smoothed $I(q,c)/c$ measured at c about 20 mg/mL. Dividing $I(q,c)/c$ by $I(q,0)/c$ gave the experimental structure factor $S(q,c)$ (eq 3).

Structure factors were calculated from the DLVO-like potentials described in eq 5, using a numerical-simulation program developed by Luc Belloni (*28*). Our fitting strategy was the simplest description of the protein−protein interactions in terms of potentials allowing to account for the experimental $S(q,c)$ curves. First, we considered the excluded volume potential and adjusted D; then, we added the electrostatic part and fitted Z; finally, if needed, we introduced the attractive component with J as the only fitted parameter and the range d set at 5 Å (a range about $D/12$ or $D/10$ was shown to account for protein fluid−fluid separation and macromolecular interactions (*20*, *29*, *30*), and D is about 80 Å).

RESULTS

Experimental Scattering Curves. The scattering curves $I(q,c)/c$ for different *Hm* MalDH concentrations are shown on Figure 1 for a selection of salt conditions. The radii of gyration extrapolated at zero protein concentration from Guinier plots (as shown on Figure 2a) are close to the value of 30−32 Å, corresponding to the tetramer (*10*). The scattering curves (for one given solvent) always coincide at large angles ($q > 0.08$ Å^{-1}), indicating that the protein

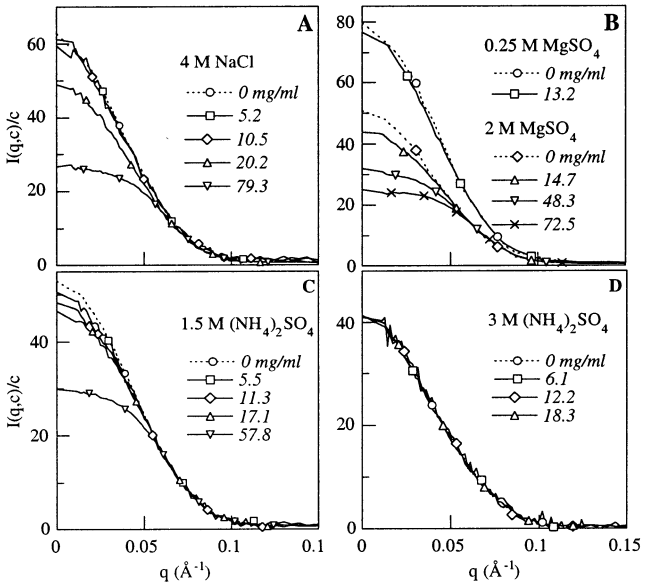

FIGURE 1: Neutron scattering of *Hm* MalDH: normalized intensities. Protein and salt concentrations are indicated on the panels. Dotted curves are the form factors extrapolated at zero protein concentration. Their amplitude depends on the protein contrast and thus on the solvent composition. The forward intensities were extrapolated according to the Guinier approximation.

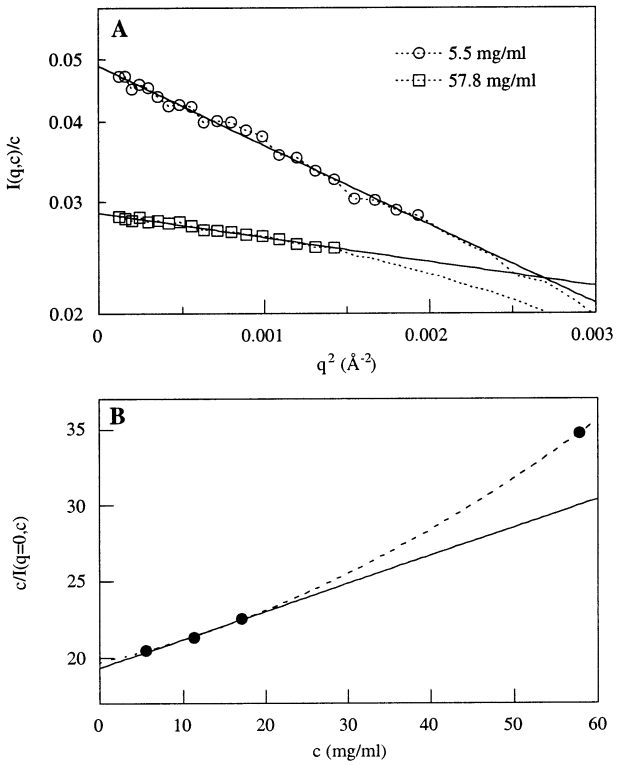

FIGURE 2: Small-angle neutron scattering: Guinier plots and determination of the second virial coefficients A_2. (a) Guinier plots allowing the determination of the apparent radii of gyration R_g^{app} and forward intensities $I(q=0,c)/c$ of *Hm* MalDH in 1.5 M $(NH_4)_2SO_4$ at 25 °C, shown for two selected protein concentrations (R_g^{app} is 29 and 19 Å at 5.5 and 57.8 mg/mL, respectively). (b) Determination of the second virial coefficient in this solvent condition: $A_2 = 3.5 \times 10^{-8}$ mol L^{-1} g^{-2} (see Materials and Methods).

quaternary structure does not change with concentration. The protein concentration dependence of the scattering curveshows, in most cases, nonideal behavior. On Figure 1, in 4 M NaCl, 2 M $MgSO_4$, and 1.5 M $(NH_4)_2SO_4$, $I(q,c)/c$ decreases at small q when c increases, indicating repulsive protein−protein interactions. Conversely, the solutions in 0.25 M $MgSO_4$ and 3 M $(NH_4)_2SO_4$ are nearly ideal since $I(q,c)/c$ does not change with c.

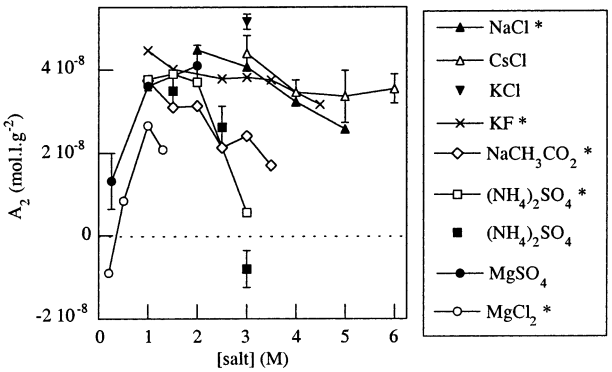

FIGURE 3: Second virial coefficients A_2 of *Hm* MalDH. Data at 20−25 °C, except * at 5 °C from (*10*).

Second Virial Coefficient. Figure 2 gives an example of the determination of the second virial coefficient A_2 from the concentration dependence of the forward intensities determined according to the Guinier approximation. On Figure 3, the A_2 values for *Hm* MalDH reveal the differences between the solvent conditions. The A_2 value is positive for a globally repulsive interactions, zero for an ideal solution, and negative for attractive interactions. Varying the temperature between 5 and 25 °C has a negligible effect on the interparticle interactions in 4 M NaCl, 1.5 M $(NH_4)_2SO_4$, and 0.2−1.3 M $MgCl_2$ (data not shown), as can be seen on Figure 3 for $(NH_4)_2SO_4$.

From A_2 values, we can distinguish two classes of solvent for *Hm* MalDH. The first comprises NaCl, CsCl, KF, KCl, and $NaCH_3CO_2$: A_2 has a positive value of about 4×10^{-8} mol L^{-1} g^{-2} that slightly decreases with the salt concentration. In $(NH_4)_2SO_4$, $MgSO_4$, and $MgCl_2$ that constitute the second class of solvent, A_2 strongly evolves between zero and 4×10^{-8} mol L^{-1} g^{-2}. A_2 rapidly increases with salt at moderate $MgCl_2$ and $MgSO_4$ and then stabilizes above 1 M. In $(NH_4)_2SO_4$, A_2 decreases above 2 M, reaching values about zero at 3 M and most probably negative values at higher salt (*Hm* MalDH precipitates at 10 mg/mL in 4 M $(NH_4)_2SO_4$).

Structure-Factor Fitting. For some salt conditions, we determined the structure factor of concentrated *Hm* MalDH solutions (up to 100 mg/mL) in order to model them. From Figure 4, an excellent agreement is obtained between experimental and calculated $S(q,c)$ using DLVO-like potentials. The results are shown only for the more concentrated sample, but the same values of D, Z, and J also account in a very satisfactory way for the structure factors at lower protein concentrations in each solvent condition. The shapes of the $S(q,c)$ are not always exactly reproduced at large angles ($q > 0.07$ Å^{-1}), because of the larger uncertainty in $S(q,c)$ or of the limits of the model potentials as reported for other proteins (*20*).

In 4 M NaCl (Figure 4a), the excluded-volume potential accounts for the protein−protein interaction. A diameter of 80 ± 2 Å gives the best fit of the experimental structure factor. The effect of an additional electrostatic potential

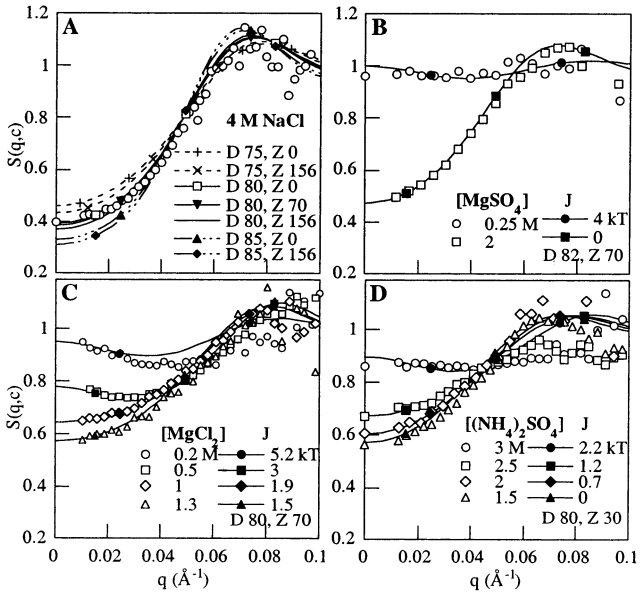

FIGURE 4: Modeling of the structure factors $S(q,c)$ of *Hm* MalDH. Open symbols, experimental curves; lines, calculated ones from the excluded-volume potential with a diameter D (in Å), the screened Coulombic potential with an effective protein charge Z and the attractive potential of depth J (in kT), and range $d = 5$ Å. Protein concentrations are, from top to bottom of each panel, as follows: (a) 98.7; (b) 13.2, 72.5; (c) 30.9, 79.6, 79.2, 85; (d) 57.8, 61, 58.1, 48.2 mg/mL.

Table 1: *Hm* MalDH Structure-Factor Modeling in Terms of DLVO-Like Excluded-Volume, Electrostatic, and Attractive Potentials[a]

salt	[salt] (M)	D (Å)	Z	J (kT)	A_2 (10^{-8} mol L^{-1} g^{-2})
NaCl	2−5	80 ± 2	1−156	0	4.5−2.6[b]
CsCl	3−6	82 ± 1	1−156	0	4.4−3.5
KCl	3	82 ± 2	1−156	0	5.1
$MgSO_4$	2	82 ± 1	1−156	0	4.1
	0.25	82	70	4 ± 0.2	1.3
$MgCl_2$	1.3	80 ± 2	70	1.5 ± 0.2	2.1[b]
	1	80	70	1.9 ± 0.1	2.6[b]
	0.5	80	70	3 ± 0.2	0.8[b]
	0.2	80	70	5.2 ± 0.2	−0.9[b]
$(NH_4)_2SO_4$	1.5	80 ± 2	1−156	0	3.5−3.9[b]
	2	80	30	0.7 ± 0.2	3.7[b]
	2.5	80	30	1.2 ± 0.1	2.6
	3	80	30	2.2 ± 0.1	0.6[b] to −0.8

[a] D and Z, protein diameter and charge. J, depth of an attractive Yukawa potential of 5 Å range. Underlined values were fixed (see text). A_2's are measured at 20−25 °C or (*b*) at 5 °C, data from ref *10*.

corresponding to an effective protein charge Z up to 156 is negligible. Because of the short-range λ_D of the screened Coulombic potential (about 1.1 Å in NaCl 4 M), the deconvolution of the two potentials is nearly impossible. Moreover, $S(q,c)$ in 4 M NaCl might also be less well fitted with a diameter of 85 Å and an additional attractive potential of depth $J = 1$ kT and range $d = 5$ Å. In 2−5 M NaCl, 3−6 M CsCl, and 3 M KCl, $S(q,c)$'s are also well fitted by using only the excluded-volume potential, with a diameter of about 80 Å or slightly larger in CsCl (see Table 1), whatever the effective charge of the protein.

In the second class of solvent, the protein−protein interactions strongly evolve with the salt concentration. For each salt type, we first attempted to fit $S(q,c)$ for the cases where repulsions were stronger with only the two repulsive potentials, and then we added an attractive component for the other conditions. In 2 M $MgSO_4$, the $S(q,c)$ is very well fitted with only the excluded-volume potential, with a diameter D of 82 ± 1 Å, Z being undefined (Figure 4b). In 0.25 M $MgSO_4$, keeping $D = 82$ Å and setting $Z = 70$, the best fit gives $J = 4 \pm 0.2$ kT for the added attractive potential. In $MgCl_2$, it is not possible to describe the $S(q,c)$ at 1.3 M (the more repulsive condition) with only the repulsive potentials (related to D and Z). For D values between 75 and 85 Å and $Z = 70$, the attractive depth J was tuned. The best fit is with $D = 80$ Å and $J = 1.5$ kT (Figure 4c). J was then the only adjustable variable at lower salt. When the salt decreases from 1.3 to 0.2 M, the attractive depth increases from 1.5 to 5.2 kT. In 1.5 M $(NH_4)_2SO_4$, $S(q,c)$ is nicely modeled with the excluded-volume term only and $D = 80$ Å. We fitted $S(q,c)$ at higher salt with an attractive potential whose depth increases from $J = 0$ at 1.5 M to $J = 2.2$ kT at 3 M (Figure 4d).

Table 1 sums up all the best values determined for the potential parameters according to our strategy. A model diameter of 80−82 Å is evaluated for the protein in solution. The effective charge is undefined due to the high salinities. The strong variations of the protein−protein interactions with the salt concentration in the second class of solvent are correlated to the presence of an attractive potential whose depth evolves with the salinity but in an opposite way in Mg salts and $(NH_4)_2SO_4$.

DISCUSSION

About the Strategy. The second virial coefficient is related to the particle distribution and reflects particle−particle interactions. The analysis of the scattering curves in an extended q domain is expected to provide richer information because modeling can be made at higher protein concentration and because particle−particle potentials of various range will affect the structure factors differently. The hypotheses of solvent continuum and spherical symmetry in DLVO potentials are reasonable since all are short-range (below 5 Å), and *Hm* MalDH is known to be globular with a roughly uniformly negatively charged surface from its high-resolution crystallographic structure (*31*). However, the DLVO approach considers ions as point charges, while it is of course evident that their size and nature affect the water structure (*32*). The Yukawa potential accounts for all the effective attractive interactions of unknown origin. Despite this simplicity, the calculated structure factors reproduce well the experimental ones and their variation with the solvent composition. But the potential system where D, Z, and J are the adjustable parameters is under-determined: a good quality of fit can be obtained with different combinations of repulsive and attractive potentials, mainly because their ranges have the same order of magnitude. In previous work, for example, on bovine serum albumin, lysozyme, or crystallins, repulsion combined with an attraction term account well for the protein−protein interactions (*20*, *29*, *33*−*35*), and the ion specificity associated to the Hofmeister effect was described by varying either the charge or the attraction term.

Table 2: Second Virial Coefficients A_2 of *Hm* MalDH and Calculated Contributions in NaCl, $(NH_4)_2SO_4$, and $MgCl_2$[a]

salt	[salt] (M)	A_2 (10^{-8} mol L^{-1} g^{-2})	$(\partial m_3/\partial m_2)_\mu$ (mol/mol)	$(\partial \mu_3/\partial m_3)_m$ (J mol^{-2})	(10^{-8} mol L^{-1} g^{-2})					
					$A_{2\,exc}$	$A_{2\,elec}$	$A_{2\,22}^{D}$	$A_{2\,23}$	$A_{2(Z=0)}$	$A_{2(Z=156)}$
NaCl	2	4.5	-38 ± 40	1784	3.3	1.5	24	-3 ± 7	0	26
	3	4.1	-54 ± 40	1634	3.3	0.7	19	-6 ± 10	-2	17
	4	3.2	-90 ± 45	1474	3.3	0.5	15	-16 ± 17	-12	4
	5	2.6	-164 ± 45	1325	3.3	0.3	13	-48 ± 29	-44	-31
$(NH_4)_2SO_4$	1	3.8	-46 ± 35	3789	3.3	0.9	33	-10 ± 17	-6	27
	1.5	3.7	-65 ± 35	2319	3.3	0.5	22	-13 ± 17	-9	13
	2	3.7	-90 ± 30	1955	3.3	0.3	17	-22 ± 22	-18	-1
	2.5	2.6	-118 ± 34	1764	3.3	0.2	13	-36 ± 33	-32	-18
	3	-0.8	-147 ± 34	1183	3.3	0.2	11	-39 ± 39	-35	-24
$MgCl_2$	0.2	-0.9	64.5 ± 20	27737	3.7	9.6	75	-143 ± 140	-138	-53
	0.5	0.85	48 ± 25	14392	3.7	2.4	33	-41 ± 53	-37	-1
	1	2.7	23 ± 20	10309	3.7	0.8	17	-7 ± 12	-3	15
	1.3	2.1	-23 ± 20	9217	3.7	0.5	13	-6 ± 14	-2	12

[a] The second virial coefficients A_2 are experimental values, as are the salt preferential binding parameters $(\partial m_3/\partial m_2)_\mu$ reported from ref *9*. $(\partial \mu_3/\partial m_3)_m$ characterizes the solvent nonideality and neglects the presence of the protein. $A_{2\,exc}$ is the estimated excluded-volume term. Electrostatic $A_{2\,elec}$ and positive Donnan contribution $A_{2\,22}^{D}$ are calculated for a protein diameter of 80 Å and charge $Z = 156$. $A_{2\,23}$ is related to preferential binding. $A_{2(Z=0)} = (\partial V_m/\partial m_p)_\mu^0/M_p^2 + A_{2\,exc} + A_{2\,23}$ corresponds to the total counterion condensation and $A_{2(Z=156)} = (\partial V_m/\partial m_p)_\mu^0/M_p^2 + A_{2\,exc} + A_{2\,elec} + A_{2\,22}^{D} + A_{2\,23}$ to the total counterion dissociation.

Hm MalDH is a highly charged protein whose solvent interactions depend strongly on the salt type and concentration. From the derivation of the second virial coefficient in terms of thermodynamic quantities (eq 9), the protein−protein interaction term $A_{2\,22}^{I}$ includes at least the positive (repulsive) excluded-volume $A_{2\,exc}$ and electrostatic $A_{2\,elec}$ contributions, and potentially also negative (attractive) ones arising, for example, from van der Waals interactions. The Donnan term $A_{2\,22}^{D}$ related to counterion dissociation is always positive. The last term, $A_{2\,23}$, results from the protein−solvent and solvent−solvent interactions and includes a Donnan contribution $A_{2\,23}^{D}$. Below, we discuss each term for *Hm* MalDH, taking into account our knowledge on its protein−solvent interactions.

Excluded-Volume Effect. Considering *Hm* MalDH as quasispherical, the structure-factor modeling allows to determine values for its diameter D between 80 and 82 Å, in good agreement with the structural dimensions of the tetramer protein. The corresponding $A_{2\,exc}$ calculated with $V_2 = 4\pi(D/2)^3/3$ are 3.6, 3.6, and 3.7 $\times 10^{-8}$ mol L^{-1} g^{-2} in NaCl, $(NH_4)_2SO_4$, and $MgCl_2$. In the companion paper, we have shown that *Hm* MalDH can be described as an invariant particle with one mole of protein strongly associated with N_1 moles of water and N_3 moles of salt. N_1 is 2000 ± 200 mol/mol in NaCl and $(NH_4)_2SO_4$ and twice this value in $MgCl_2$. N_3 is zero in $(NH_4)_2SO_4$, 55 in NaCl, and 85 in $MgCl_2$ (*9*). Considering a compact and incompressible spherical solvated particle, from these values and the partial molal volumes $\bar{V}_i$, we can calculate solvated-protein volumes as $(\bar{V}_2+N_1\bar{V}_1+N_3\bar{V}_3)/N_A$, corresponding diameters D of 75, 76, and 81 Å and $A_{2\,exc}$ of 3.0, 3.0, and 3.8 $\times 10^{-8}$ mol L^{-1} g^{-2} in NaCl, $(NH_4)_2SO_4$, and $MgCl_2$, respectively. Without solvation, the calculation would lead to $D = 67$ Å and $A_{2\,exc} = 2.1 \times 10^{-8}$ mol L^{-1} g^{-2}, emphasising the importance of the solvation shell.

The diameters determined by the structure-factor modeling are not sufficiently precise (±2 Å) to establish any correlation between the particle volumes and the salt-dependent amounts of associated solvent. The mean $A_{2\,exc}$ in NaCl, $(NH_4)_2SO_4$, and $MgCl_2$, from the structure factor modeling and from the composition of the solvated protein are reported in Table 2. The excluded-volume term largely accounts for the positive A_2 values of the first class of salts. However, $A_{2\,exc}$ can be smaller than the measured A_2, for example, in 2−3 M NaCl. More generally, the excluded-volume term does not account for the drop of A_2 with the salinity, even in the first class of salts.

Electrostatic Effect and Donnan Terms. The maximum values of $A_{2\,elec}$ calculated in NaCl, $(NH_4)_2SO_4$, and $MgCl_2$ for an effective protein charge Z of 156 are reported in Table 2. The electrostatic repulsive interactions are not entirely screened in our salt conditions. The sum of the excluded-volume and electrostatic terms correlates fairly well with the decrease of the experimental A_2 with salt in 2−4 M NaCl, 1−2 M $(NH_4)_2SO_4$ (Table 2), and CsCl (not shown). A description of a highly charged *Hm* MalDH appears suitable. If our data can be modeled in some cases with only these two repulsive potentials, their underestimation or a missing term compensated by additional attractive ones is not excluded. Counterion dissociation induces a global positive contribution to A_2, $A_{2\,22}^{D} + A_{2\,23}^{D}$, which reduces to $V_m^0Z^2/4M_2^2m_3$ in 1:1 salts and $V_m^0Z^2/6M_2^2m_3$ in 1:2 and 2:1 salts, when dropping all nonideality terms. Since $A_{2\,23}^{D}$ is an indiscernible part of $A_{2\,23}$, the Donnan effect will be treated below.

Attractive Protein−Protein Interactions from Protein-Induced Solvent Redistribution. A deep attractive component is required to model the structure factors at low $MgCl_2$ and $MgSO_4$ and high $(NH_4)_2SO_4$. For these salt conditions, the A_2 value is decreased, indicating interparticle attraction, but without providing insights on its origin. The A_2 expression in terms of thermodynamic quantities shows a negative contribution $A_{2\,23}$ related to the preferential salt binding parameter $(\partial m_3/\partial m_2)_\mu$ when a cosolvent is present in solution (eq 10). We derived $A_{2\,23}$ for native *Hm* MalDH in NaCl, $(NH_4)_2SO_4$, and $MgCl_2$, from the data of Ebel et al. (*9*) (Table 2). It has to be noticed that only the experimentally measured parameter $(\partial m_3/\partial m_2)_\mu$ is used and that a structural interpretation of the data (in terms of bound solvent molecules for example) is not required. Because a_{33} varies as $1/m_3$ in a

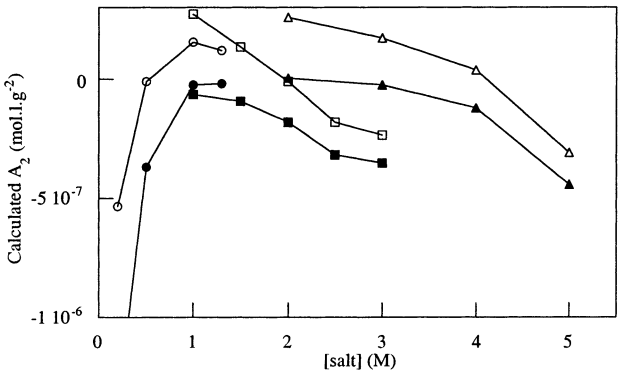

FIGURE 5: Calculated second virial coefficients of *Hm* MalDH. $A_{2(Z=0)}$ (filled symbols) for total counterion condensation and $A_{2(Z=156)}$ (open symbol) for total counterion dissociation in NaCl (triangle), $(NH_4)_2SO_4$ (square), and $MgCl_2$ (circle), considering excluded-volume, electrostatic, and Donnan effects and the contribution from the protein-induced solvent redistribution.

first approximation, the effect of $(\partial m_3/\partial m_2)_\mu$ on $A_{2\,23}$ is strongly modulated by the salt concentration: similar absolute values give rise to a larger effect at low salt and a smaller one at high salt. For example, for $|(\partial m_3/\partial m_2)_\mu|$ values of 65 mol/mol, $A_{2\,23}$ values of -143, -13, and -8×10^{-8} mol L^{-1} g^{-2} are derived in 0.2 M $MgCl_2$, 1.5 M $(NH_4)_2SO_4$, and 3.2 M NaCl, respectively. It is obvious that $A_{2\,23}$—relative to preferential binding—and $A_{2\,22}{}^{D}$—the maximum Donnan term—correspond to large contributions of opposite sign, which partially compensate. We have shown in the companion paper that salt binding and counterion dissociation (Donnan effect, which appears as negative salt binding) cannot be distinguished. We calculate in Table 2 a global second virial coefficient for two limiting cases: $A_{2(Z=156)} = (\partial V_m/\partial m_2)_\mu{}^0/M_2{}^2 + A_{2\,\mathrm{exc}} + A_{2\,\mathrm{elec}} + A_{2\,22}{}^{D} + A_{2\,23}$ and $A_{2(Z=0)} = (\partial V_m/\partial m_2)_\mu{}^0/M_2{}^2 + A_{2\,\mathrm{exc}} + A_{2\,23}$, corresponding to total dissociation and total condensation of the counterions, respectively. Figure 5 displays how they evolve in $MgCl_2$, $(NH_4)_2SO_4$, and NaCl. The experimental A_2 values are between these two calculated values, except for the high values of $|(\partial m_3/\partial m_2)_\mu|$. The calculated A_2 show larger variations than the experimental ones. The consequences of the combination of the Donnan and solvent effects are overestimated. This could be due to errors in the measurements of the preferential binding parameters. More likely, the estimation of $A_{2\,22}{}^{I}$ in terms of excluded volume and electrostatic repulsion is probably inaccurate and must depend in an other way on the solvent composition. Our data suggest a threshold under which the protein−solvent interactions would not really influence the protein−protein interactions.

It is clear, however, that the calculated A_2 qualitatively reproduce the experimental evolution of A_2 with the salt concentration. The strong decreases of A_2 are clearly correlated to large positive or negative values of $(\partial m_3/\partial m_2)_\mu$, as can be seen at high $(NH_4)_2SO_4$ and low $MgCl_2$. In these salt conditions, the structure-factor modeling requires a strong attractive protein−protein potential. The result of protein-induced solvent redistribution appears as an attractive potential in the protein−protein interactions, except for the particular case $(\partial m_3/\partial m_2)_\mu = 0$. $(\partial m_3/\partial m_2)_\mu$ can be interpreted in terms of solvent binding sites. If N_1 and N_3 are the numbers of water and salt binding sites, $(\partial m_3/\partial m_2)_\mu = (N_3 - E_3) - N_1(m_3/m_1)$, where E_3 arises from the dissociation of the counterions (Donnan term) in the case of a polyelectrolyte macromolecule. In the case of strong binding sites, the composition of the solvated particle does not depend on the solvent composition, as was described for *Hm* MalDH (*9*). Thus, at low salt, we expect $(N_3 - E_3)/N_1 > (m_3/m_1)$ and $(\partial m_3/\partial m_2)_\mu > 0$; at intermediate salt, $(N_3 - E_3)/N_1 = (m_3/m_1)$ and $(\partial m_3/\partial m_2)_\mu = 0$; at higher salt, $(N_3 - E_3)/N_1 < (m_3/m_1)$ and $(\partial m_3/\partial m_2)_\mu < 0$. Thus, protein−protein attractive contribution could be expected at low and high salt as seen in $MgCl_2$. In the case of ammonium sulfate, where $(N_3 - E_3)$ is close to zero, the attractive contribution is expected only at high salt concentration.

A positive value of $(\partial m_3/\partial m_2)_\mu$ corresponds to a stabilizing effect of the salt on protein. Indeed, μ_2 decreases when the salt concentration increases from the given solvent condition, because $(\partial \mu_2/\partial m_3)_m = -(\partial m_3/\partial m_2)_\mu \cdot (\partial \mu_3/\partial m_3)_m$, and $(\partial \mu_3/\partial m_3)_m$ is always positive. Thus, $(\partial m_3/\partial m_2)_\mu$ gives insights into the effect of changes in the solvent composition on protein stabilization and conformational equilibrium (*36*−*39*). The fact that positive and negative values of $(\partial m_3/\partial m_2)_\mu$ have the same effect on A_2 or $d\Pi/dc$ can be understood intuitively as explained in the following. The effect of increasing the protein concentration is now studied for a given solvent composition. The result of the favorable interaction of protein with a solvent component will be the same whether it is the principal solvent or the cosolvent. An unequal distribution of the solvent components in the solution is entropically unfavorable and destabilizes the solution. It destabilizes both water and salt in the solvent (eq 12, with a lower A_2 values arising from the negative $A_{2\,23}$ contribution). Thus, the destabilized solvent tends to exclude the protein. The consequence is an effective protein−protein attraction, which is unrelated to specific macromolecule interactions and is measured in A_2 or in the structure factor from the spatial distribution of the macromolecule in solution. We can understand qualitatively that the consequence of contact between proteins is a global decrease of the amount of perturbed solvent, and thus a decrease of the volume where water and cosolvent are not distributed homogeneously. For negative A_2, a protein concentration is expected where $\mu_1 - \mu_{1\,\mathrm{bulk}}$ and $\mu_3 - \mu_{3\,\mathrm{bulk}}$ will reach positive values. The solution becomes unstable and molecular changes leading to different solvent interactions or phase separations are expected. Protein precipitation is one of the possible logical consequences of negative A_2 values.

This study brings to the fore the symmetrical effect of water and cosolvent enrichment or impoverishment in the protein solvation shell on the weak protein−protein interactions. The effect of protein preferential hydration on protein solubility is documented. The salting out-efficiency of a series of salts was found to correspond to increasing values of preferential hydration of proteins. The solutes that increase the surface tension of the solution—leading to nonspecific hydration—decrease protein solubility (*36*). The depletion of large particles as poly(ethylene glycol) explains their precipitating effect (*35*, *40*, *41*). On the other hand, the effects on protein solubility of positive values of salt binding are not considered. It is perhaps because positive values of $(\partial m_3/\partial m_2)_\mu$, related to numerous and not so weak protein−solute interactions, are not often measured. We note, however, that the low guanidinium hydrochloride concentra-

tions corresponding to positive values of $(\partial m_3/\partial m_2)_\mu$ are avoided for the optimum reconstitution of denatured protein to avoid protein aggregation (*42*, *43*). Also, slightly positive values of $(\partial m_3/\partial m_2)_\mu$ reported for β-lactoglobulin in 0.5 M $MgCl_2$ or glycine, pH 5.1, correspond to a decreased solubility compared to 1 M (*44*, *45*). The aggregation of detergent-solubilized membrane proteins below the critical micelle concentration could also be related to the destabilizing unequal distribution of the detergent between the solution and the solvation shell.

Halophily and Protein−Protein Interactions. Thermodynamics and our results on *Hm* MalDH show that protein-induced solvent redistribution could be an essential and determining component of effective weak protein−protein interactions. Any positive or negative contrast of the solvation shell with the bulk solvent can induce an effective attractive term in protein−protein interactions. High protein solubility thus requires the solvent to be as "neutral" as possible, avoiding any water or cosolvent enrichment in the protein solvation shell. For *Hm* MalDH, the solvent conditions for which $(\partial m_3/\partial m_2)_\mu$ and its effect on A_2 are close to zero, as in KCl and NaCl, correspond to globally repulsive protein−protein interactions ($A_2 \gg 0$) and high solubility. To be active, stable, and soluble in high salt are major challenges facing proteins in the nearly salt-saturated cytoplasm of extreme halophilic microorganisms. Halophilic proteins are characterized by a high content of acidic residues. From crystallography, most of the acidic residues of *Hm* MalDH are localized in patches on its surface (*31*), the others taking part of multiple salt bridges at subunit interfaces (*46*). From solution and crystallographic studies, weak and strong ion-binding sites on the highly charged surface of the folded protein stabilize the folded protein at high salt (*9*, *46*). From the present work, the high salt concentration in the solvation shell in high KCl or NaCl appears also to be required to avoid water enrichment on the protein surface that could lead to protein−protein attraction. The marked acidic character of the surface of halophilic proteins constitutes the major feature of the molecular adaptation to high salt. From this study, it is related to the necessary requirement of macromolecule solubility for life.

ACKNOWLEDGMENT

Thanks are due to Dr. L. Belloni (CEA Saclay, France) for providing the program for structure factor modeling and advice, to the staff of the ILL, and to Dr. P. Vachette for his help at LURE (Orsay, France).

REFERENCES

1. Minton, A. P. (2001) *J. Biol. Chem. 276*, 10577−10580.
2. Delaye, M., and Tardieu, A. (1983) *Nature 302*, 415−417.
3. Vérétout, F., Delaye, M., and Tardieu, A. (1989) *J. Mol. Biol. 205*, 713−728.
4. George, A., and Wilson, W. W. (1994) *Acta Crystallogr. D50*, 361−365.
5. George, A., Chiang, Y., Guo, B., Arabshahi, A., Cai, Z., and Wilson, W. W. (1997) *Methods Enzymol. 276*, 100−110.
6. Guo, B., Kao, S., McDonald, H., Asanov, A., Combs, L. L., and Wilson, W. W. (1999) *J. Cryst. Growth 196*, 424−433.
7. Ducruix, A., Guilloteau, J. P., Riès-Kautt, M., and Tardieu, A. (1996) *J. Cryst. Growth 168*, 28−39.
8. Georgalis, Y., and Saenger, W. (1998) *Curr. Top. Cryst. Growth Res. 4*, 1−62.
9. Ebel, C., Costenaro, L., Pascu, M., Faou, P., Kernel, B., ProustDe Martin, F., and Zaccai, G. (2002) *Biochemistry 41*, 13234−13244.
10. Ebel, C., Faou, P., and Zaccai, G. (1999) *J. Cryst. Growth 196*, 395−402.
11. Costenaro, L., Zaccai, G., and Ebel, C. (2001) *J. Cryst. Growth 232*, 102−113.
12. Derjaguin, B. V., and Landau, L. (1941) *Acta Physicochim. URSS 14*, 633−662.
13. Verwey, E. J. W., and Overbeek, J. T. G. (1948) *Theory of Stability of Lyophobic Colloids*, Elsevier, Amsterdam.
14. Hansen, J. P., and McDonald, I. R. (1986) *Theory of Simple Liquids*, 2nd ed., Academic Press, London.
15. Eisenberg, H. (1976) *Biological Macromolecules and Polyelectrolytes in Solution*, Clarendon Press, Oxford.
16. Eisenberg, H. (1981) *Q. Rev. Biophys. 14*, 141−172.
17. Solovyova, A., Schuck, P., Costenaro, L., and Ebel, C. (2001) *Biophys. J. 81*, 1868−1880.
18. Tardieu, A. (1994) in *Neutron and Synchrotron Radiation for Condensed Matter Studies* (Baruchel, J., Hodeau, J. L., Lehmann, M. S., Regnard, J. R., and Schlenker, C., Eds.) pp 145−160, Les Editions de Physique, Springer-Verlag, Berlin.
19. Belloni, L. (2000) *J. Phys.: Condens. Matter 12*, R549−R587.
20. Tardieu, A., Le Verge, A., Malfois, M., Bonneté, F., Finet, S., Riès-Kautt, M., and Belloni, L. (1999) *J. Cryst. Growth 196*, 193−203.
21. Scatchard, G. (1946) *J. Am. Chem. Soc. 68*, 2315−2319.
22. Casassa, F. E., and Eisenberg, H. (1964) *Adv. Protein Chem. 19*, 287−395.
23. Tanford, C. (1961) *Physical Chemistry of Macromolecules*, Wiley, New York.
24. Cendrin, F., Chroboczek, J., Zaccai, G., Eisenberg, H., and Mevarech, M. (1993) *Biochemistry 32*, 4308−4313.
25. Guinier, A., and Fournet, G. (1955) *Small-Angle Scattering of X-Rays*, Wiley, New York.
26. Luzzati, V., and Tardieu, A. (1980) *Annu. Rev. Biophys. Bioeng. 9*, 1−29.
27. Jacrot, B., and Zaccai, G. (1981) *Biopolymers 20*, 2413−2426.
28. Belloni, L. (1991) in *Neutron, X-ray and Light Scattering: Introduction to an Investigative Tool for Colloidal and Polymeric Systems*, Proceedings of the European Workshop on Neutron, X-Ray and Light Scattering as an Investigative Tool for Colloidal and Polymeric Systems, Bombannes, France, 27 May−2 June, 1990 (Lindner, P., and Zemb, T., Eds.) pp 135−155, North-Holland, Amsterdam.
29. Malfois, M., Bonneté, F., Belloni, L., and Tardieu, A. (1996) *J. Chem. Phys. 105*, 3290−3300.
30. Peyre, V., Spalla, O., Belloni, L., and Nabavi, M. (1997) *J. Colloid Interface Sci. 187*, 184−200.
31. Dym, O., Mevarech, M., and Sussman, J. L. (1995) *Science 267*, 1344−1346.
32. Collins, K. D. (1997) *Biophys. J. 72*, 65−76.
33. Minton, A. P. (1995) *Biophys. Chem. 57*, 65−70.
34. Bonneté, F., Malfois, M., Finet, S., Tardieu, A., Lafont, S., and Veesler, S. (1997) *Acta Crystallogr. D53*, 438−447.
35. Finet, S., and Tardieu, A. (2001) *J. Cryst. Growth 232*, 40−49.
36. Timasheff, S. N. (1993) *Annu. Rev. Biophys. Biomol. Struct. 22*, 67−97.
37. Parsegian, V. A., Rand, R. P., and Rau, D. C. (1995) *Methods Enzymol. 259*, 43−94.
38. Timasheff, S. N. (1998) *Proc. Natl. Acad. Sci. U.S.A. 95*, 7363−7367.
39. Parsegian, V. A., Rand, R. P., and Rau, D. C. (2000) *Proc. Natl. Acad. Sci. U.S.A. 97*, 3987−3992.
40. Arakawa, T., and Timasheff, S. N. (1985) *Biochemistry 24*, 6756−6762.
41. Budayova, M., Bonneté, F., Tardieu, A., and Vachette, P. (1999) *J. Cryst. Growth 196*, 210−219.
42. Schellman, J. A. (1990) *Biophys. Chem. 37*, 121−140.
43. Vandenbroeck, K., Martens, E., D'Andrea, S., and Billiau, A. (1993) *Eur. J. Biochem. 215*, 481−486.
44. Arakawa, T., Bhat, R., and Timasheff, S. N. (1990) *Biochemistry 29*, 1914−1923.
45. Arakawa, T., and Timasheff, S. N. (1987) *Biochemistry 26*, 5147−5153.
46. Richard, S. B., Madern, D., Garcin, E., and Zaccai, G. (2000) *Biochemistry 39*, 992−1000.

BI025830Z